Electro-optic properties of GaInAsSb/GaAs quantum well for high-speed integrated optoelectronic devices

Jiri Thoma, Baolai Liang, Charles Reyner, Tomasz Ochalski, David Williams, Stephen P. Hegarty, Diana Huffaker, and Guillaume Huyet

Citation: Appl. Phys. Lett. **102**, 013120 (2013); doi: 10.1063/1.4775371
View online: http://dx.doi.org/10.1063/1.4775371
View Table of Contents: http://aip.scitation.org/toc/apl/102/1
Published by the American Institute of Physics

Electro-optic properties of GaInAsSb/GaAs quantum well for high-speed integrated optoelectronic devices

Jiri Thoma,[1,2] Baolai Liang,[3] Charles Reyner,[3] Tomasz Ochalski,[1,2] David Williams,[1,2] Stephen P. Hegarty,[2] Diana Huffaker,[3] and Guillaume Huyet[1,2]
[1]*CAPPA, Cork Institute of Technology, Cork, Ireland*
[2]*Tyndall National Institute, Lee Maltings, Cork, Ireland*
[3]*California NanoSystems Institute and Department of Electrical Engineering, UCLA, Los Angeles, California 90095, USA*

(Received 3 September 2012; accepted 21 December 2012; published online 11 January 2013)

The electro-optic properties of strained GaInAsSb/GaAs quantum wells (QWs) are investigated. A single QW p-i-n sample was grown by molecular beam epitaxy with antimony (Sb) pre-deposition technique. We numerically predict and experimentally verify a strong quantum confined Stark shift of 40 nm. We also predict a fast absorption recovery times crucial of high-speed optoelectronic devices mainly due to strong electron tunneling and thermionic emission. Predicted recovery times are corroborated by bias and temperature dependent time-resolved photoluminescence measurements indicating ($\leq$30 ps) recovery times. This makes GaInAsSb QW an attractive material particularly for electroabsorption modulators and saturable absorbers. © *2013 American Institute of Physics*. [http://dx.doi.org/10.1063/1.4775371]

The demand for higher reliability, lower heat dissipation, and reduced manufacturing cost is driving the adoption of more highly integrated photonic devices.[1,2] The material systems based on InP substrate, InGaAsP/InP in particular,[3,4] are still dominant in present backbone networks, but their higher cost hinders deployment in metropolitan and local area networks with much higher device density.[5,6] Among other disadvantages, a low electron conduction band (CB) confinement of around 100 meV[4,7,8] and poor thermal conductivity of InP alloy both result in the need for active cooling.[7] Poor integration with other optical elements and low refractive index contrast in a Distributed Bragg reflector (DBR) lasers are additional drawbacks.[8,9] In contrast, the GaAs materials have significant attractions as emitters at 1310 nm. Lattice mismatch, however, limits the maximum indium(In) content and thus the longest achievable wavelength in two-dimensional (2D) growth mode. The highest emission wavelength reported for an InGaAs quantum well (QW) laser was at 1240 nm for a highly strained material[10] with lasing threshold current density per well as low as 70 A/cm^2 for broad area lasers.[11] Recently, much effort has been focused on exploring the GaInAsN/GaAs QW where adding small amounts of nitrogen(N) leads to favorable changes in band alignment and pushes the emission wavelength towards 1310 nm.[12–14] An impact of N incorporation is the deterioration of the optical properties as defect induced nonradiative recombination (NRR) increases with increasing N concentration,[15] although recent work has shown that the addition of minimal amount of N ($\leq$0.5%) together with a post-growth annealing treatment (680 °C, 10 min) in GaInAsN QW hinder from formation of N-N pairs and clusters and thus do not lead to reduction in the intrinsic gain of the active region.[16] While the NRR could be advantageous for fast saturable aborbers (SAs) and electroabsorption modulators (EAMs) as an additional carrier recombination process,[17,18] it is largely detrimental for the gain properties, with lasing threshold densities remaining relatively high. The lowest lasing threshold current density reported was 211 A/cm^2 or 300, 400, and 940 A/cm^2 from single[19] to quadruple[20] QW lasers. This has motivated exploration of low temperature growth, combined with Sb surfactant, allowing the increase of In concentration in 2D growth without reaching the critical thickness.[21] In addition, the incorporation of Sb in GaInAs leads to bandgap reduction that is favorable for the extension of the emission wavelength.[22] Furthermore, as the Sb diminishes the strain relaxation (i.e., the plastic relaxation by generation of dislocations and elastic relaxation by surface undulation[22]) the optical quality increases, improving the device performance. The reported threshold current density of double QW lasers was as low as 125 A/cm^2 per well.[23] These properties make a GaInSbAs material advantageous over GaInNAs.

In this work, we have studied the electro-optic properties of a single GaInAsSb QWs grown on a GaAs(100) substrate by a VEECO GEN 930 III-V molecular beam epitaxy system. The p-i-n sample intrinsic region thickness w = 206 nm, consisting of a 6 nm GaInAsSb QW within undoped 100 nm GaAs buffers, delimited by the upper p-doped and bottom n-doped $Al_{0.3}Ga_{0.7}$ As claddings on an n-doped GaAs substrate [Table I]. The QW was grown at a temperature of 425 °C, while the GaAs buffers and AlGaAs cladding layers at a substrate temperature of 580 °C. Both In and Ga growth rates were set at 0.15 ML/s. The group V flux beam equivalent pressure (BEP) was set at BEP = 4.0×10^{-7} Torr for Sb_2 and BEP = 2.0×10^{-6} Torr for As_2, respectively. To improve the QW quality, the sample was grown using the Sb pre-deposition method, where a 25 s Sb-soak was conducted before the QW growth.[24] Thereby, we achieved the In- and Sb-contents within the InGaAsSb QW to be 30% and 7%, respectively. Photoluminescence (PL) spectra showed a peak emission wavelength of 1165 nm with a full-width half maximum (FWHM) of 50 nm. To test the electro-absorption performance of the GaInAsSb QW material, the p-i-n wafer was processed into a set of mesas

TABLE I. Schematic description of the GaInAsSb QW p-i-n structure with detailed dimensions and doping.

Material	Thickness [nm]	Doping [cm^{-3}]
GaAs	100	1×10^{19}
p-$Al_{0.3}$GaAs	100	1×10^{18}
p-$Al_{0.3}$GaAs	50	5×10^{17}
GaAs	100	
$Ga_{0.7}In_{0.3}As_{0.93}Sb_{0.07}$ QW	6	
GaAs	100	
n-$Al_{0.3}$GaAs	50	5×10^{17}
n-$Al_{0.3}$GaAs	100	1×10^{18}
GaAs buffer	100	1×10^{18}
n+ GaAs substrate		

and metal contacts with an inner diameter of 50 μm were applied. The good optical quality and thus low defect density was confirmed by measurable electroluminescence at a current density of 6 A/cm^2.

In the first experiment, the exciton shift of the p-i-n sample due to the quantum confined Stark effect (QCSE) was studied as a function of the reverse bias voltage (RBV) applied. The photocurrent (PC) absorption technique was employed using a supercontinuum laser source (Fianium, 400 nm to 2100 nm coverage) and monochromator with sub-nanometer resolution to optically excite the sample. On the detection side, a voltage source (Keithley 2400) was used for sample biasing, while a shunt resistor in series with the sample served as a current-to-voltage convertor for the input of a lock-in amplifier. The excitation wavelength was varied around the expected ground state exciton peak, i.e., from 1120 nm up to 1240 nm, and the external bias was varied from 0.0 V down to −3.5 V, which corresponded (with the built-in potential $V_{built} = 1.12$ V) to a total internal electric field strength varying from 54 kV/cm up to 224 kV/cm. A strong QCSE shift of 40 nm for the exciton peak can be seen, the prominent absorption peak observable at zero applied bias is gradually weakened, until it is no longer visible from −2.5 V bias and lower [Fig. 1(a)]. The biggest experimental absorption extinction ratio [Fig. 1(b)] of 12 dB has been observed for a 35-40 nm detuning toward longer wavelengths, i.e., around 1210 nm, at external bias of −3.5 V. These features were numerically investigated by k·p simulations [Fig. 2(a)] of GaInAsSb/GaAs QWs for different electric fields. Due to the field induced conduction band tilting, the electron wavefunction has a tail extending out through the triangular GaAs barrier (for F ≥ 100 kV/cm), which results into field-induced broadening of this weakly bound exciton peak. Further, the calculated QCSE shift shows quadratic dependence on the total electric field and the approximately 40 nm shift seen in the simulations is in agreement with the shift observed in our experiment [Fig. 2(b)].

For high-speed operation in integrated optoelectronic devices, rapid absorption and gain recovery are crucial. All the carrier dynamics are driven by the radiative recombination (RR) and NRR originating either from the GaInAsSb QW or GaAs barriers and next by the carrier escape processes making QW recovery depending both on temperature and external bias. Those carriers, which escaped out of the

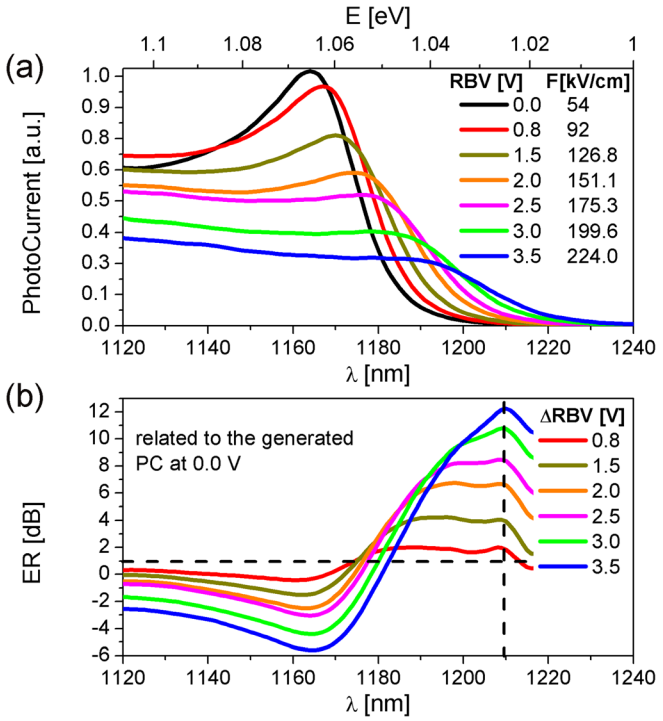

FIG. 1. (a) Room temperature photocurrent absorption spectra demonstrate 40 nm shift of GaInAsSb QW exciton under −3.5 V bias applied from initial 1165 nm at 0.0 V. (b) Over 12 dB extinction ratio of an optical absorption has been observed at 35-40 nm longer wavelengths.

QW, can be either captured back by the QW, radiatively recombine inside the barriers or be accelerated by an electric field across the intrinsic region and be collected by the top and bottom contacts. These collected carriers then contribute to the PC signal. A schematic diagram showing all the carrier processes is sketched [Fig. 3]. In order to study the carrier dynamics and to better understand the significance of each of

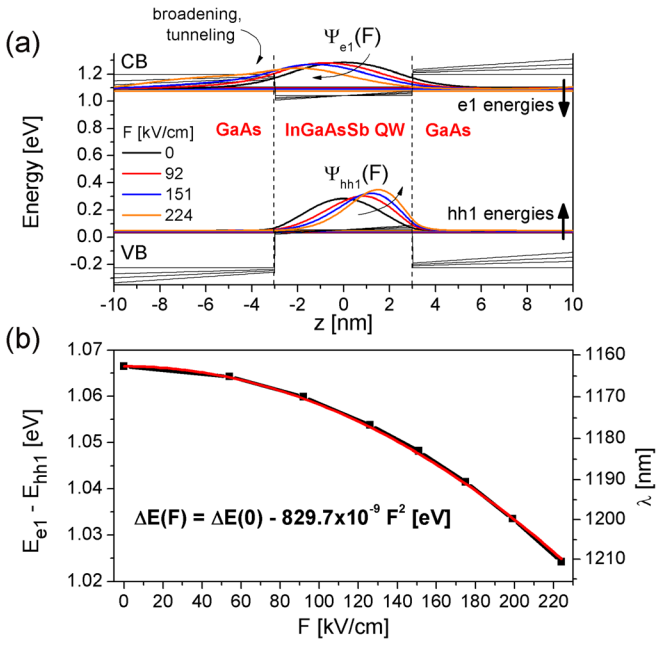

FIG. 2. (a) k·p method calculation of QCSE under external electric field (0-224 kV/cm) corresponding to the experiment performed showing a field induced electron tunneling through the triangular GaAs barrier. (b) A quadratic dependence of a peak wavelength position on increasing total electric field showing 40 nm redshift.

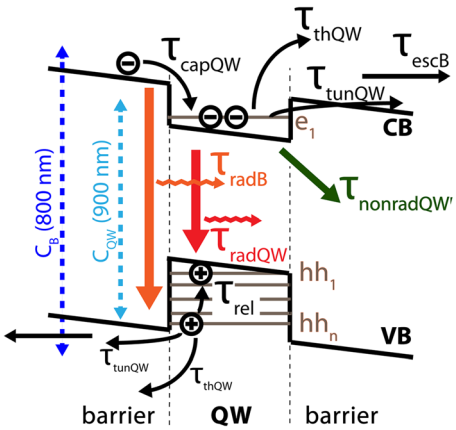

FIG. 3. Schematic of the GaInAsSb/GaAs QW model used for carrier relaxation and escape mechanisms.

the individual contributions, we performed a set of time-resolved photoluminescence (TRPL) experiments as a function of bias and temperature for two distinct excitation energies; (a) 1.551 eV (800 nm), i.e., above the GaAs bandgap energy and (b) 1.3786 eV (900 nm), i.e., below the GaAs bandgap energy.

In the first, below GaAs excitation experiment, the external bias (electric field) was varied from 1.12 V (0 kV/cm) down to −1.50 V (127 kV/cm), where the forward bias of 1.12 V goes against the p-i-n built-in voltage and corresponds to a flat band. A confocal geometry with 300 fs pulsewidth, tunable mode-locked Ti:Sapphire laser was used to pump the structure and a monochromator with a Hamamatsu streak camera was used on the detection side. This measurement was performed at 14 K (using a closed-loop helium cryostat), where both thermionic emission and NRR processes are significantly suppressed, and thus the QW carrier density depends only on the RR and the field induced tunneling. With decreasing bias voltage, we can observe [Fig. 4(a)] that, first, the carrier lifetime is slowly decreasing up to the external bias of −0.5 V; second, a abrupt lifetime decrease occurs between the external biases of −0.5 V and −1.0 V. This is a consequence of two features. At an excitation wavelength of 900 nm, we generate electron-hole pairs only inside the QW, electrons in the ground (e1) state (due to low conductive band offset the only supported electron state inside the GaInAsSb QW) and holes in the highest excited state. However, with very low energy offset (14.6 meV) to the GaAs barrier, the holes can tunnel through the thin triangular GaAs barrier even at low electric field strength and escape. The rest relax to the heavy hole ground state (hh1) and radiatively recombine with the available e1-electrons. The hole tunneling probability increases in line with increasing electric field and it is responsible for the QW PL lifetime shortening. For electric fields ($F \geq 100$ kV/cm), the tunneling process is activated even for the e1-electrons and it leads to the PL decay time as short as 26 ps at −1.5 V (127 kV/cm). This is in direct agreement with both the PC measurement and the k·p simulation above. In the second experiment, the NRR and thermal escape effects on the carrier dynamic behavior have been determined. We measured the carrier lifetime at different temperatures from 10 K up to 290 K with no external bias applied, thus under the constant built-in

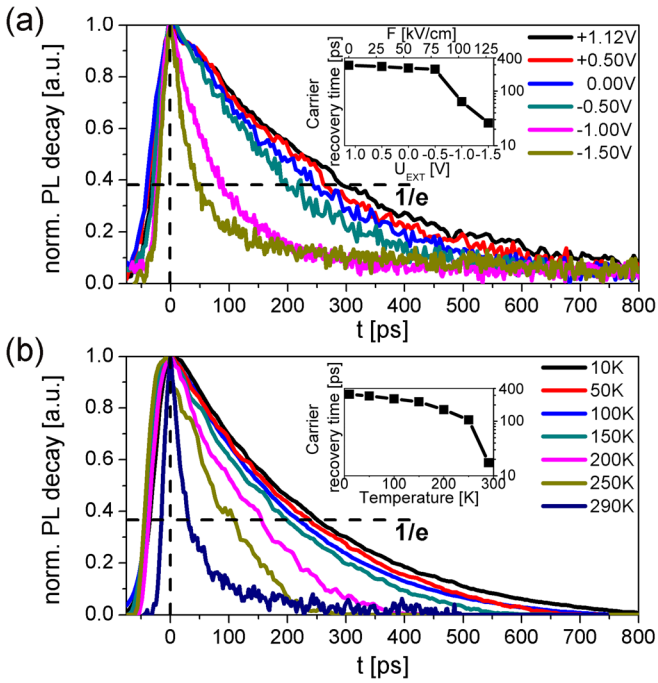

FIG. 4. The below GaAs bandgap (900 nm) excitation carrier dynamic TRPL measurements (a) first, bias dependent (+1.12 V to −1.50 V) TRPL decay traces showing a tunneling at electric fields ($F \geq 100$ kV/cm). (b) Second, temperature dependent (10–290 K) TRPL decay traces under a constant built-in electric field of 54 kV/cm. The insets show the extracted PL lifetimes in semilog scale.

electric field with strength of 54 kV/cm [Fig. 4(b)]. With increasing temperature, the thermally activated defects inside the QW lead to NRR. This feature is relatively weak, indicative of a low defect density, and the main process responsible for faster carrier dynamics is the hole thermionic emission. With rising temperature, the PL lifetime decreases more rapidly and the PL decay time reaches 30 ps at room temperature [Fig. 4(b) inset]. In general, once the carriers escape to the GaAs matrix, they are either recaptured by the QW or accelerated by the electric field and contribute to the PC. While recapture is certainly possible under low electric field, with increasing electric field bias its probability rapidly decreases in favor of generated PC.

The above GaAs bandgap excitation at 14 K is qualitatively different from the below bandgap excitation experiment. After carrier generation inside the GaAs matrix, the QW capture process competes with the GaAs RR and the field dependent escape from barriers to the external circuitry, thus (in contrast to below GaAs excitation) making the QW radiative lifetime very sensitive to the applied bias for all cases, i.e., from 1.12 V [Fig. 5(a)]. The carriers captured by the QW subsequently radiatively recombine (after rapid relaxation), with only the highest energy state holes tunneling (similarly to the below barriers excitation) as a QW escape mechanism. Further, abrupt decrease in the QW radiative lifetime occurs at lower biases (≤ -1.0 V) and for both excitation energies the QW radiative lifetimes have comparable values of 26 ps (900 nm) and 36 ps (800 nm) at the external voltage of −1.5 V. For completeness, in the last temperature dependent above bandgap excitation measurement [Fig. 5(b)], we can see the carrier dynamic behavior as a mixture of above processes. Under the built-in electric

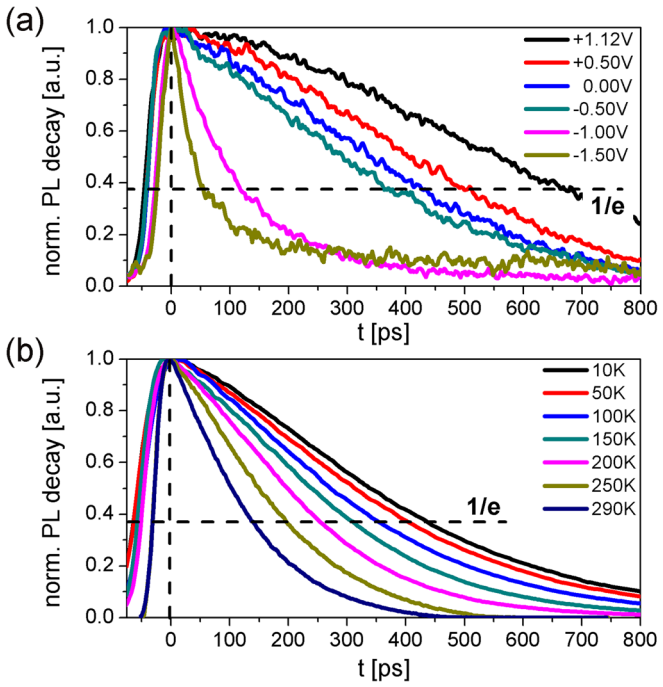

FIG. 5. The above GaAs bandgap (800 nm) excitation carrier dynamic TRPL measurements (a) first, bias dependent (+1.12 V to −1.50 V) TRPL decay traces showing a tunneling at electric fields (F ≥ 100 kV/cm). (b) Second, temperature dependent (10–290 K) TRPL decay traces under built-in electric field of 54 kV/cm).

field, the QW capture is competing with the carriers escape process. Those holes captured by the QW relax into the hh1 state and radiatively recombine. With increasing temperature, the QWs carrier lifetime is gradually shortened as the thermionic hole emission gradually drains the carriers from the highest excited state and reduces their relaxation rate into the hh1 state.

In this work, we have investigated the electro-optic properties of the GaInSbAs/GaAs QW p-i-n structure. First, by utilizing a PC absorption spectra technique we report on 40 nm redshift incurred by a strong QCSE. By bias and temperature dependent time-resolved measurement of PL we have analyzed all, i.e., (non)radiative, relaxation, and escape mechanisms driving the carrier dynamics. Comparing the experimental results to the theoretical calculations based on a self-consistent 8-band k·p algorithm, we were able to interpret the observed 40 nm redshift in the QW exciton absorption together with its fast recovery. We have shown that both loss of exciton sharpness and fast dynamic at low temperature (26 ps) are particularly caused by electron tunneling through the GaAs barrier even under low external bias of −1.5 V. Fast dynamic (30 ps) is also achieved at room temperature with zero bias applied, due to hole thermionic emission. As a mixture of tunneling and thermal processes, we could expect further increase of escape rates, taking into account the thermally assisted tunneling. These properties make GaInSbAs QW attractive material for a high-speed saturable absorber and/or electro-absorption modulator in an integrated device as a high-speed operation is achieved at low voltage favorable of a low power consumption.

This work was supported by the Science Foundation Ireland (SFI) Strategic Research Cluster, PiFAS, under Contract No. 07/SRC/I1173. The authors also gratefully acknowledge the financial support of United States Department of Defense (Grant NSSEFF N00244-09-1-0091).

[1]Y. Cheng, J. Pan, Y. Wang, F. Zhou, B. Wang, L. Zhao, H. Zhu, and W. Wang, IEEE Photon. Technol. Lett. **21**, 356 (2009).
[2]Ch. Sun, B. Xiong, J. Wang, P. Cai, J. Xu, J. Huang, H. Yuan, Q. Zhou, and Y. Luo, J. Lightw. Technol. **26**, 1464 (2008).
[3]G. P. Agrawal, *Fiber-Optic Communication Systems* (Wiley Series Hardcover, 2010)
[4]M. S. Alias, S. M. Mitani, and F. Maskurity, Optik **123**, 1051 (2012).
[5]J. S. Harris, Semicond. Sci. Technol. **17**, 880 (2002).
[6]G. Adolfsson, S. Wang, M. Sadeghi, J. Bengtsson, A. Larsson, J. J. Lim, V. Vilokkinen, and P. Melanen, IEEE J. Quantum Electron. **44**, 607 (2008).
[7]M. Kondow, K. Uomi, A. Niwa, T. Kitatani, S. Watahiki, and Y. Yazawa, Jpn. J. Appl. Phys. **35**, 1273 (1996).
[8]M. Kondow, T. Kitatani, S. Nakatsuka, M. C. Larson, K. Nakahara, Y. Yazawa, M. Okai, and K. Uomi, IEEE J. Sel. Top. Quantum Electron. **3**, 719 (1997).
[9]A. Yu. Egorov, A. E. Zhukov, and V. M. Ustinov, J. Electron. Mater. **30**, 477 (2001).
[10]L. W. Sun and H. H. Lin, Appl. Phys. Lett. **83**, 1107 (2003).
[11]P. Sundgren, J. Berggren, P. Goldman, and M. Hammar, Appl. Phys. Lett. **87**, 071104 (2005).
[12]N. Tansu and L. J. Mawst, Appl. Phys. Lett. **82**, 1500 (2003).
[13]N. Tansu, J.-Y. Yeh, and L. J. Mawst, Appl. Phys. Lett. **83**, 2512 (2003).
[14]S. Wu and L. Wan, J. Appl. Phys. **110**, 123109 (2011).
[15]R. Fehse, S. Tomic, A. R. Adams, S. J. Sweeney, E. P. O'Reilly, A. Andreev, and H. Riechert, IEEE J. Sel. Top. Quantum Electron. **8**, 801 (2002).
[16]J. W. Ferguson, P. Blood, P. M. Smowton, H. Bae, T. Sarmiento, J. S. Harris, N. Tansu, and L. J. Mawst, IEEE J. Quantum Electron. **47**, 870 (2011).
[17]O. Anton, C. S. Menoni, J. Y. Yeh, L. J. Mawst, J. M. Pikal, and N. Tansu, IEEE Photon. Technol. Lett. **17**, 953 (2005).
[18]F. Schttiger, D. Bauer, J. Demsar, T. Dekorsy, J. Kleinbauer, D. H. Sutter, J. Puustinen, and M. Guina, Appl. Phys. B **106**, 605–612 (2012).
[19]N. Tansu, N. J. Kirsch, and L. J. Mawst, Appl. Phys. Lett. **81**, 2523 (2002).
[20]H. Zhao, S. M. Wang, Q. X. Zhao, M. Sadeghi, and A. Larsson, J. Cryst. Growth **311**, 1723 (2009).
[21]D. Jiang, Y.-H. Qu, H.-Q. Ni, D.-H. Wu, Y.-Q. Xu, and Z.-Ch. Niu, J. Cryst. Growth **288**, 12 (2006).
[22]J. C. Harmand, L. H. Li, G. Patriarche, and L. Travers, Appl. Phys. Lett. **84**, 3981 (2004).
[23]T. Kageyama, T. Miyamoto, M. Ohta, T. Matsuura, Y. Matsui, T. Furuhata, and F. Koyama, J. Appl. Phys. **96**, 44 (2004).
[24]Y. H. Qu, D. S. Jiang, D. H. Wu, Z. C. Niu, and Z. Sun, Chin. Phys. Lett. **22**, 2088 (2005).